Research Article

Erik Heinz*, Christian Eling, Markus Wieland, Lasse Klingbeil and Heiner Kuhlmann

Development, Calibration and Evaluation of a Portable and Direct Georeferenced Laser Scanning System for Kinematic 3D Mapping

DOI 10.1515/jag-2015-0011
received July 30, 2015; accepted October 23, 2015.

Abstract: In recent years, kinematic laser scanning has become increasingly popular because it offers many benefits compared to static laser scanning. The advantages include both saving of time in the georeferencing and a more favorable scanning geometry. Often mobile laser scanning systems are installed on wheeled platforms, which may not reach all parts of the object. Hence, there is an interest in the development of portable systems, which remain operational even in inaccessible areas. The development of such a portable laser scanning system is presented in this paper. It consists of a lightweight direct georeferencing unit for the position and attitude determination and a small low-cost 2D laser scanner. This setup provides advantages over existing portable systems that employ heavy and expensive 3D laser scanners in a profiling mode.

A special emphasis is placed on the system calibration, i. e. the determination of the transformation between the coordinate frames of the direct georeferencing unit and the 2D laser scanner. To this end, a calibration field is used, which consists of differently orientated georeferenced planar surfaces, leading to estimates for the lever arms and boresight angles with an accuracy of mm and one-tenth of a degree. Finally, point clouds of the mobile laser scanning system are compared with georeferenced point clouds of a high-precision 3D laser scanner. Accordingly, the accuracy of the system is in the order of cm to dm. This is in good agreement with the expected accuracy, which has been derived from the error propagation of previously estimated variance components.

***Corresponding author: Erik Heinz,** Institute of Geodesy and Geoinformation, University of Bonn, Nußallee 17, 53115 Bonn, Germany, e-mail: e.heinz@igg.uni-bonn.de
Christian Eling, Markus Wieland, Lasse Klingbeil, Heiner Kuhlmann, Institute of Geodesy and Geoinformation, University of Bonn, Germany, e-mail: c.eling@igg.uni-bonn.de, m.wieland@igg.uni-bonn.de, l.klingbeil@igg.uni-bonn.de, heiner.kuhlmann@uni-bonn.de

Keywords: Kinematic Laser Scanning, Portable System, Direct Georeferencing, Calibration, Variance Component Estimation, Evaluation

1 Introduction

In the modern information society, there is a growing interest in digital three-dimensional data of urban and rural areas in order to meet applications in the field of documentation, inventory management, planning, visualization and navigation. A well-known example for the use of spatial 3D data is the reconstruction of 3D city models.

Terrestrial laser scanning (TLS) has been proved to be an efficient measurement technique for the acquisition of spatial 3D data as it is characterized by high speed, high accuracy and high resolution. Principally, TLS is based on the fully automatic sensing of an object from a fixed position by using a laser beam. However, a major disadvantage in the acquisition of large or complex objects is that the laser scanner has to be moved to different positions in order to completely cover the object and to provide a sufficient point density. The subsequent problem of registrating the individual scans in a joint coordinate frame is usually solved by using ground control points or automated registration algorithms such as the ICP (Iterative Closest Point) [2]. Many applications also require a georeferenced point cloud. This can be realized by measuring the coordinates of the ground control points, e. g. with GNSS. Both the registration and the georeferencing of TLS lead to increased costs, which affect the economic efficiency.

In contrast to TLS, kinematic laser scanning does not require separate working steps for the registration or georeferencing of individual scans. It can be classified in the context of mobile mapping because the laser scanner is moved through the object space and spatial 3D data is collected in motion. The georeferencing of

the laser scanner is done on-the-fly by using additional sensors [11, 15, 16, 19, 36, 45] or information from the object space [11, 45]. Thus, the scans are georeferenced automatically, which implicates enormous time and cost savings.

The different options for the position and attitude determination of a moving laser scanner are summarized in [33]. The first option is the utilization of supplementary sensors such as GNSS, IMUs, odometers or inclinometers. These sensors are rigidly connected to the laser scanner on a jointly used platform in the form of a multi sensor system. Another opportunity to provide position and attitude information is to track the laser scanner with a georeferenced instrument, e. g. a total station, a laser tracker or cameras. This, however, has the drawback that a permanent line of sight between the laser scanner and the tracking instrument is required. Both variants are common as direct georeferencing. The second option is based on the use of information from the object space, e. g. ground control points or geometric shapes, which is known as indirect georeferencing. Besides the time saving in the georeferencing, also the quality of the point clouds can be improved due to kinematic laser scanning because the distances between the laser scanner and the object can be maintained short, favorable angles of incidence can be ensured and the point clouds show a more homogeneous point density without data gaps.

Within this work, a mobile laser scanning system is presented, which consists of a lightweight direct georeferencing unit and a small low-cost 2D laser scanner on a jointly used platform (Section 2). The direct georeferencing unit is in-house developed and equipped with differential GPS, an IMU and a magnetometer. It provides precise estimates of the position and attitude of the platform. A special feature of the system is that it is portable and makes use of a small low-cost 2D laser scanner. This provides advantages over existing portable laser scanning systems that employ heavy and expensive 3D laser scanners in a profiling mode [11, 25]. Its compact and lightweight design benefits the mobility and allows for a flexible data acquisition even in inaccessible areas where wheeled platforms are inapplicable due to soft ground or narrow passages [25].

Besides the benefits, the presented mobile laser scanning system also implicates particular requirements. Principally, the individual sensors provide their observations at different moments in time and with a different temporal resolution. Therefore, a precise time synchronization is required in order to relate position, attitude and object space information to the same moment in time. This is realized by using electrical trigger pulses (Section 3).

Also the mutual installation position of all sensors on the platform must be accurately determined because each sensor provides its observations in its own coordinate frame. This problem is known as geometric system calibration. The determination of the six degrees of freedom, i. e. three translations (lever arms) and three rotations (boresight angles), between the direct georeferencing unit and the 2D laser scanner is a key issue of this paper (Section 4). These calibration parameters are primarily unknown but assumed to be time-invariant. Consequently, they have to be determined only once before using of the system. This is realized by means of a special calibration field, which consists of differently orientated georeferenced planar surfaces. The calibration field also allows for an estimation of variance components of the observations of the mobile system, which can be used for an accuracy analysis.

Finally, some point clouds of the mobile laser scanning system are evaluated (Section 5). Deviations from reference point clouds are examined and compared to the expected system accuracy, which has been derived from the error propagation of the previously estimated variance components. This contribution concludes with a resume and an outlook on future developments (Section 6).

2 System Design

The mobile laser scanning system, which has been developed within this work, is composed of different sensors for the georeferencing of the moving platform (direct georeferencing unit) and the acquisition of object space information (2D laser scanner). The primarily use of lightweight equipment enables a human being to carry the system. Hence, it is characterized by improved mobility in areas with hard environmental conditions like soft ground or narrow passages where the use wheeled platforms is not possible [25]. The entire system has a dimension of some decimeters (GPS baseline on top measures circa 90 cm) and a weight of about 8.5 kg (without batteries), which is mainly due to the metallic frame (Figure 1). The design was not optimized to be ultra-light but to be flexible. The total weight of less than 1.5 kg for the direct georeferencing unit, the GPS antennas and the 2D laser scanner would allow for a lighter setup and offers an advantage over existing portable laser scanning systems that employ heavy 3D laser scanners in a profiling mode [11, 25]. The following sections contain a brief description of the system components. In [7–9] more details on the direct georeferencing unit can be found.

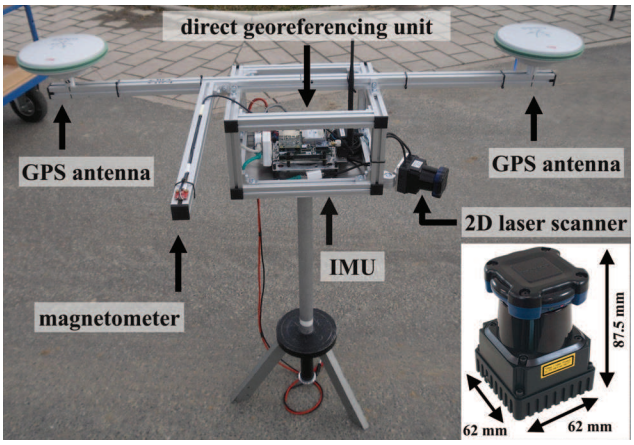

Figure 1: Portable laser scanning system composed of a lightweight direct georeferencing unit (differential GPS, IMU, magnetometer) and a small 2D laser scanner.

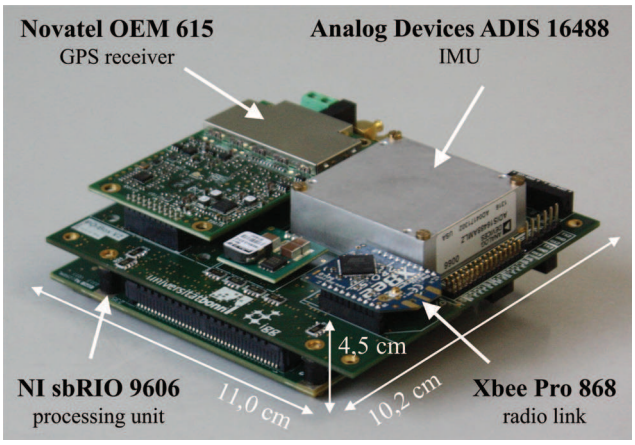

Figure 2: Small and lightweight direct georeferencing unit for the position and attitude determination (without GPS antennas, HMC magnetometer and power supply) [7, 8].

2.1 Direct Georeferencing Unit

The direct georeferencing unit[1] is a small and lightweight system for the real-time determination of the position and the attitude of a micro aerial vehicle (Figure 2). Within this work, it was adopted for the mobile laser scanning system. The dimensions of this unit are 11.0 cm × 10.2 cm × 4.5 cm and it has a weight of approximately 240 g (without GPS antennas and power supply). It is composed of a geodetic grade dual-frequency GPS receiver (Novatel OEM 615) and a low-cost single-frequency GPS receiver (u-blox LEA6T). These are connected to two external geodetic grade dual-frequency GPS antennas (Leica AS10). Additionally, the unit contains a tactical grade MEMS-IMU (Analog Devices ADIS 16488) with three-axis gyroscopes, accelerometers, a magnetometer and a barometer. In this sensor combination the magnetometer is intended to provide information for the heading determination. However, the observations of the magnetometer are too much affected by ferromagnetic materials and electric currents in the vicinity of the sensor, which cause non-negligible distortions even if the sensor is well calibrated [3]. Therefore, an additional magnetometer (Honeywell HMC 5883L) was mounted on a side arm where the influences are less significant (Figure 1).

The position and attitude determination of the platform is realized via three consecutive steps. These are part of the in-house developed trajectory estimation software:

- RTK-GPS position,
- GPS compass,
- GPS/IMU integration.

The position determination is mainly based on the observations of the dual-frequency GPS receiver and those received from a master station via a radio link (Xbee Pro 868). This allows for a precise RTK-GPS solution within an extended Kalman filter, leading to position estimates with an accuracy of < 5 cm and a temporal resolution of 10 Hz.

Due to the magnetic distortions, the magnetometer does not allow for a sub-degree heading determination. This is why the GPS baseline on top of the mobile system is added to serve as a GPS compass. The problem concerning the integration of the GPS baseline is that only single-frequency observations are available whose ambiguity resolution typically takes several minutes [35]. For this reason, the magnetometer readings and the accelerations of the IMU are used to calculate an approximate attitude in order to shrink the search space for the ambiguity resolution [9]. Thus, the ambiguities can usually be fixed to their integer values within the first epoch.

The attitude determination is carried out in a quaternion based extended Kalman filter by using the observations of the IMU and the magnetometer. In addition, the RTK-GPS positions and the baseline parameters of the GPS compass are introduced to this filter via a loosely-coupled approach to simultaneously estimate both position and attitude. The result of this GPS/IMU integration is a georeferencing

1 The direct georeferencing unit is currently under development at the Institute of Geodesy and Geoinformation at the University of Bonn as part of the project "Mapping on Demand (MoD)", funded by the DFG (Deutsche Forschungsgemeinschaft), project number 1505.

at 100 Hz with a smoothed position and an attitude with an accuracy of < 0.5° –1°. Note, that roll and pitch can be determined more accurately than the heading because the heading strongly depends on the inaccurate magnetometer if the baseline is missing while roll and pitch can be derived very precisely from gravity variations. All processing steps are run on the direct georeferencing unit in real-time by using a real-time processing unit (National Instruments sbRIO 9606). This also allows for an online data visualization.

2.2 2D Laser Scanner

The scanning device is a 2D time-of-flight laser scanner Hokuyo UTM-30LX-EW with a 270° field of view, 0.25° angular resolution, 30 m guaranteed range and 40 Hz scanning rate. Its main characteristics are the small dimensions (62 mm × 62 mm × 87.5 mm) and the low weight (210 g, without cable). The 2D laser scanner is mounted in a way that it records vertical profiles (Figure 1).

The accuracy of the sensor is specified in the order of mm to cm on behalf of the manufacturer [20]. This could be confirmed in an own experiment where differently colored planar surfaces were measured at varying distances. The analysis of repeated distance readings clearly shows a constant precision of about 5 mm in the close range < 10 m and a slope of approximately 5 mm per 10 m between 10 m and 30 m (Figure 3). The results do not depend on the object color because of the infrared laser beam ($\lambda = 905$ nm).

Furthermore, systematic effects of the 2D laser scanner were discovered. During a static long-term measurement of a planar surface (duration 60 min, distance 3.3 m), a slow drift of the distance readings d in the order of 4 mm to 6 mm became visible, subsiding after half an hour (Figure 4). The authors suggest that it is a consequence of the increasing temperature inside the device [22]. This has been verified for a similar 2D laser scanner in [44]. During static test measurements yet another systematic effect of the 2D laser scanner was discovered: The distances are measured systematically too short at regular angular intervals of 6°–7°. The device provides distance measurements at fixed angular steps of 0.25°. The angles are generated synthetically under the assumption of a constant angular velocity of the sensor head and considered to be the same for each revolution. After averaging the distances for the single angular steps, the object points are located closer to the 2D laser scanner at fixed angular increments of 6°–7° (cf. red dots in Figure 5). This phenomenon occurred whenever using the device, but it could not be explained.

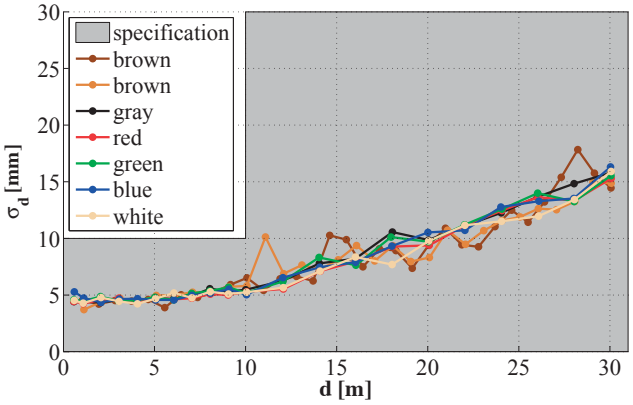

Figure 3: Empirical repeated accuracy σ_d of the Hokuyo UTM-30LX-EW as a function of the distance d for different object colors.

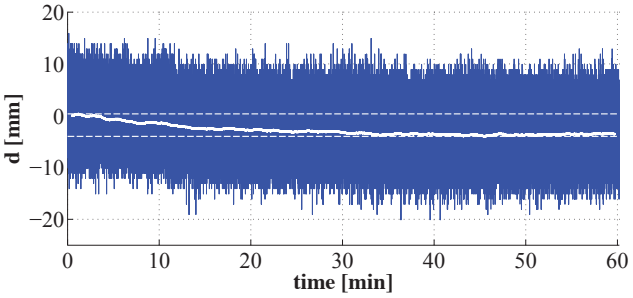

Figure 4: Drift of the Hokuyo UTM-30LX-EW during a long-term measurement due to increasing temperature.

3 Time Synchronization

In kinematic applications, the correct time synchronization of the different sensors is very important to precisely relate all observations to the same moment in time. This is usually realized with electrical trigger pulses, but can also be carried out by employing software-based correlation techniques, see e. g. [6, 24, 41, 46]. For the presented laser scanning system a hardware-based solution was chosen.

In the present case, all sensors and the real-time processing unit are connected to an FPGA (Field Programmable Gate Array), which continuously receives the observations of all sensors. Additionally, it gets a PPS signal (pulse per second) from the dual-frequency GPS receiver. This pulse serves as the timekeeping element for the internal clock of the platform, which starts different tasks on the processor that instantaneously request the observations of the direct georeferencing unit from the FPGA and calculate the position and attitude (Section 2.1). The estimates obtain the current system time as timestamp. The 2D laser scanner has its own pulse, which is

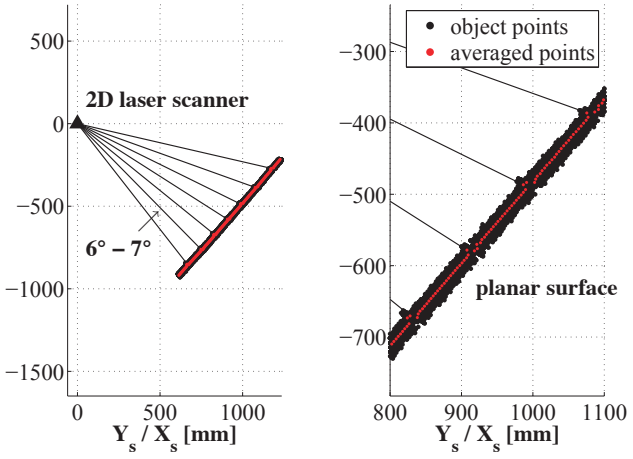

Figure 5: Systematically too short measured distances of the Hokuyo UTM-30LX-EW at fixed angular intervals.

triggered whenever the device starts a new revolution. When receiving this pulse, the FPGA starts a task on the processor which requests the observation data of the subsequent profile and stores it with the current system time as timestamp. By means of interpolation, the time of measurement can be determined for each scanned point with associated position and attitude of the platform.

4 Geometric System Calibration

4.1 Problem Formulation

As shown in Figure 6, the direct georeferencing unit and the 2D laser scanner operate in different coordinate frames. The aim of the geometric system calibration is the determination of the transformation between these frames in order to spatially link the 2D laser scanner observations to the position and attitude estimates. In the present case, a total of four individual coordinate frames must be distinguished:

- s-frame (scanner-frame),
- b-frame (body-frame),
- n-frame (navigation-frame),
- e-frame (earth-frame).

The observations of the 2D laser scanner, i. e. distance d and angle a, are provided in the s-frame. The object points have to be transformed to the b-frame because the estimates of the direct georeferencing unit are referred to this frame. The b-frame is rigidly connected to the moving platform (e. g. the center of the IMU) and usually aligned with its main directions of movement (forward, leftward, upward). The determination of the transformation between these two frames is the objective of the geometric system calibration (Figure 6). It can be described by six unknown parameters: three translations Δx, Δy and Δz (lever arms) and three rotations α, β and γ (boresight angles)

$$\begin{bmatrix} x_b \\ y_b \\ z_b \end{bmatrix} = \boldsymbol{R}_s^b\left(\alpha,\beta,\gamma\right) \underbrace{\begin{bmatrix} d\cdot\cos a \\ d\cdot\sin a \\ 0 \end{bmatrix}}_{\begin{bmatrix} x_s & y_s & z_s \end{bmatrix}^T} + \begin{bmatrix} \Delta x \\ \Delta y \\ \Delta z \end{bmatrix}. \tag{1}$$

If these six parameters are known, the observed object points can be transformed to the b-frame and subsequently to a superior coordinate frame by adding the estimates of the direct georeferencing unit. The attitude, i. e. roll ϕ, pitch θ and heading ψ, provides the transformation between b-frame and n-fame, which is aligned with the north, east and up direction. The GPS position can finally be used to transfer the object coordinates to the e-frame, which coincides with WGS84 / ITRF. The latter is a five parameter transformation which uses the Cartesian e-frame coordinates t_x, t_y and t_z and the approximate ellipsoidal latitude L and longitude B of the platform. Together with Equation (1) this leads to

$$\begin{bmatrix} x_e \\ y_e \\ z_e \end{bmatrix} = \begin{bmatrix} t_x \\ t_y \\ t_z \end{bmatrix} + \boldsymbol{R}_n^e\left(L,B\right)\boldsymbol{R}_b^n\left(\phi,\theta,\psi\right)\begin{bmatrix} x_b \\ y_b \\ z_b \end{bmatrix}. \tag{2}$$

Obviously, all quantities for the transformation of local object points (s-frame) into global object points (e-frame) can be observed with the aid of the mobile laser scanning system, except for the lever arms and boresight angles between b-frame and s-frame. Note, that these six parameters are assumed to be not variable in time, and hence have to be determined only once before using the mobile system.

4.2 Selection of the Calibration Method

To solve the problem of the geometric system calibration several calibration techniques have been developed, which often make use of reference geometries, predominantly planar surfaces.

In [42] an approach is presented which utilizes a special reference geometry consisting of five differently orientated planar surfaces. These are georeferenced in a superior coordinate frame by using a laser tracker with scanning module (Leica T-Scan) and then statically scanned with a 2D laser

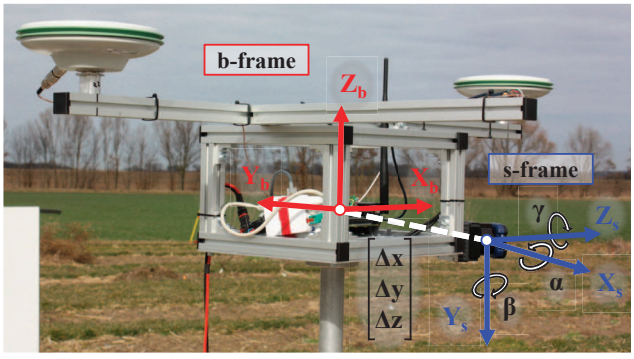

Figure 6: Mutual position (Δx, Δy, Δz) and orientation (α, β, γ) between s-frame und b-frame on the platform.

scanner of a multi sensor system. The b-frame on the platform is realized by bores. Thus, it can be determined in the laser tracker frame by utilizing a corner cube reflector. The laser tracker takes over the task of the direct georeferencing unit used within this work. An identity condition between the planes and the 2D laser scanner points can be formulated. This constraint contains the six unknown calibration parameters, which can be estimated in an adjustment with associated accuracies. This approach is also applied in [6] in a slightly modified version.

The authors found this approach to be suitable for the geometric system calibration of the mobile laser scanning system because it meets the requirements adequately. The scanning of planar surfaces has the advantage that the spatial information of the laser scanner can be fully exploited. This is not the case when using ground control points [19, 43, 45]. In addition, ground control points cannot be measured directly and have to be extracted from the point cloud with a certain loss of accuracy. Planar surfaces are advantageous due to their simple parametrization, but all parametrizable geometric shapes, e. g. cylinders or spheres, can be used. A direct measurement of the six degrees of freedom is also excluded because there are no physical reference points available for s-frame and b-frame.

Various other publications address the determination of the geometric system calibration by using planar surfaces. In [15, 16] an approach is presented which does not use single points but entire scan profiles on planar surfaces. These are approximated by best fitting lines and again identity conditions are formulated. Also in the context of airborne laser scanning, scanned object points are linked to planar surfaces on the earth's surface, e. g. rooftops, in order to determine the geometric system calibration. In [40] an approach for the determination of the boresight angles is presented which ignores the lever arms, but in exchange it integrates an additive constant for the laser scanner as intrinsic calibration parameter. The reference objects do not have to be georeferenced which makes it a self-calibration approach, see also [12, 29]. A positioning free self-calibration method for mobile laser scanning systems is presented in [26]. It only needs the attitude of the platform and the laser scanner readings to determine the boresight angles. No georeferencing of the planes is required, too.

Another completely different self-calibration approach, which does not require any geometric structure like planes, has been described in [30, 39]. The point cloud of an arbitrary test site is represented as realization of a probability density function. The calibration parameters are obtained by maximizing the density's quadratic Rényi entropy, which quantifies the compactness of the point cloud.

In [24, 37, 41] free test field environments with differently orientated planar surfaces (e. g. building facades) or cylindrical objects are scanned kinematically several times in opposite directions or from different sides. As a result, residual deviations in the boresight angles affect the shape of the point clouds with different algebraic sign. By minimizing the occurring deviations, e. g. a tilting of a facade or a horizontal shift of a cylindric object, the calibration parameters can be improved.

4.3 Parameter Estimation

Within this contribution, a special calibration technique for the determination of the transformation between s-frame and b-frame was chosen. It is based on the approach presented in [42] and was modified for the present case. The approach makes use of differently orientated georeferenced planar surfaces, which serve as control objects (Figure 7, left). The principles of the methodology will be illustrated in detail below, whereas the practical realization and the results will be discussed in Section 4.5.

First, the calibration planes have to be georeferenced in the superior coordinate frame. This can be realized with a 3D TLS, which has been localized in the e-frame by using ground control points. After that, the planes are scanned with the 2D laser scanner of the mobile system. A constraint g_1 can be formulated that the georeferenced object points of the mobile laser scanning system must satisfy the associated normalized plane equation (Figure 7, right)

$$g_1 : \begin{bmatrix} x_e \\ y_e \\ z_e \end{bmatrix}^T \begin{bmatrix} n_x \\ n_y \\ n_z \end{bmatrix} - 1 \stackrel{!}{=} 0. \tag{3}$$

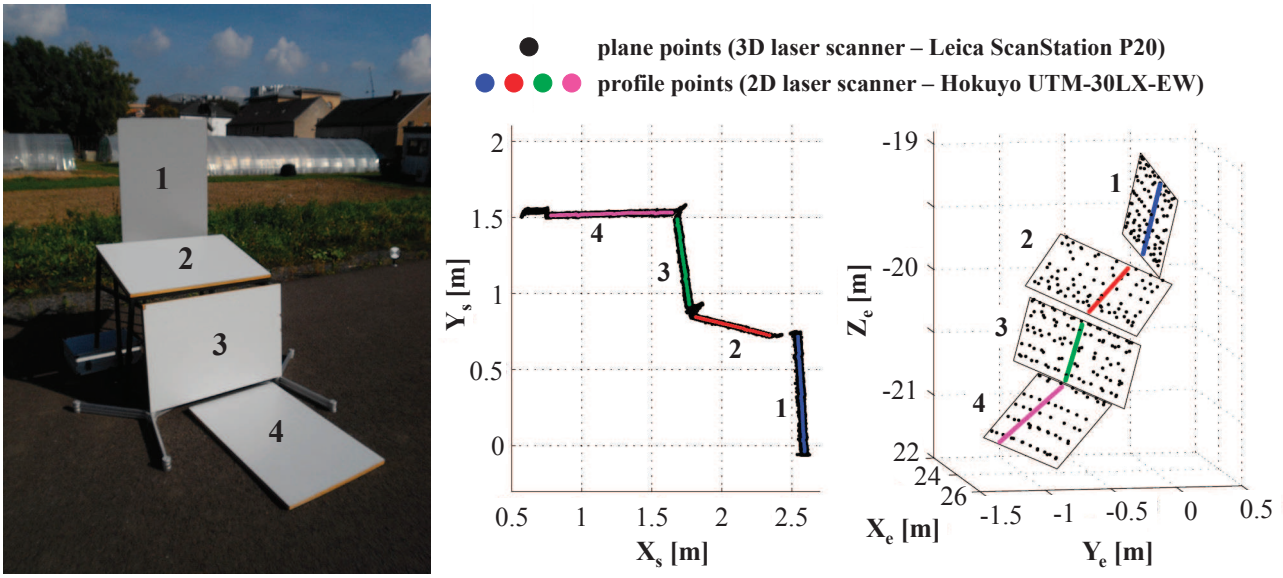

Figure 7: Planar surfaces for the geometric system calibration (left). The planes are determined in the superior coordinate frame (e-frame) and subsequently scanned with the 2D laser scanner (s-frame) of the mobile laser scanning system (middle). The sensed profiles must lie on the planes (right), which can be formulated as an adjustment constraint. The transformation parameters between s-frame and b-frame remain unknown within this constraint.

By inserting Equations (1) and (2) into Equation (3), a functional relationship is obtained, which can be used as observation equation in a total least square approach (Gauß Helmert model), providing estimates for the unknown calibration parameters (Δx, Δy, Δz, α, β, γ) and their accuracies. Within this adjustment, also the normals of the different planar surfaces (n_x^i, n_y^i, n_z^i) are treated as parameters, whereas almost all other quantities (d, a, ϕ, θ, ψ, t_x, t_y, t_z) are treated as observations. Due to their little influence on the error propagation, the ellipsoidal latitude B and longitude L can be treated as constant values.

Since the calibration parameters and the plane parameters cannot be separated from each other, a singularity exists in the related normal equation system. This singularity can be eliminated by introducing the georeferenced plane point coordinates of the TLS to the adjustment, expressed by transformed slope distance s_e, horizontal direction r_e and vertical angle z_e. This leads to a second constraint g_2

$$g_2: \begin{bmatrix} s_e \cdot \sin z_e \cdot \cos r_e \\ s_e \cdot \sin z_e \cdot \sin r_e \\ s_e \cdot \cos z_e \end{bmatrix}^T \begin{bmatrix} n_x \\ n_y \\ n_z \end{bmatrix} - 1 \overset{!}{=} 0. \tag{4}$$

In the adjustment, the transformed TLS observations are treated as observations to take into account that the reference planes cannot be assumed to be error-free. Another opportunity would be to estimate the plane normals in a preadjustment step and use them as constant values.

Since the observation equations are non-linear with respect to the parameters, they have to be linearized and approximate values for the parameters are required. This leads to an iterative solution of the related normal equation system. The strict solution of the Gauß Helmert model has been addressed in many publications, see e. g. [28, 31, 32], and therefore a more detailed illustration is omitted.

However, it should be mentioned that in the present case the Gauß Helmert model is transformed into a Gauß Markov model to deal efficiently with the numerically large number of observations [21, 47]. This leads to the following algorithm for the estimation of the parameters $\tilde{\mathbf{x}}$ and their accuracies $\Sigma_{\tilde{x}\tilde{x}}$. The parameters are calculated iteratively by estimating parameter updates $\Delta\tilde{\mathbf{x}}$ for the initial assumed approximate parameter values $\mathbf{x}_0$

$$\Delta\tilde{\mathbf{x}} = \left(\mathbf{A}^T\left(\mathbf{B}\Sigma_{ll}\mathbf{B}^T\right)^{-1}\mathbf{A}\right)^{-1}\mathbf{A}^T\left(\mathbf{B}\Sigma_{ll}\mathbf{B}^T\right)^{-1}\mathbf{w} \tag{5}$$

$$\tilde{\mathbf{x}} = \mathbf{x}_0 + \Delta\tilde{\mathbf{x}} \tag{6}$$

$$\Sigma_{\tilde{x}\tilde{x}} = \left(\mathbf{A}^T\left(\mathbf{B}\Sigma_{ll}\mathbf{B}^T\right)^{-1}\mathbf{A}\right)^{-1}. \tag{7}$$

The matrices **A** and **B** contain the partial derivatives of g_1 and g_2 with respect to the parameters and the observations. The item **w** is the vector of discrepancies, which contains the evaluation of the functional relationship. It is always calculated with the currently valid parameter values and the adjusted observations, which are derived by adding residuals **v** to the original observations **l**

$$\mathbf{A} = \left.\frac{\partial g_i\left(\mathbf{x},\mathbf{l}\right)}{\partial \mathbf{x}}\right|_{\mathbf{x}_0,\mathbf{l}+\mathbf{v}_0} \qquad \mathbf{B} = \left.\frac{\partial g_i\left(\mathbf{x},\mathbf{l}\right)}{\partial \mathbf{l}}\right|_{\mathbf{x}_0,\mathbf{l}+\mathbf{v}_0} \tag{8}$$

$$\mathbf{w} = -g_i\left(\mathbf{l}+\mathbf{v}_0,\mathbf{x}_0\right)+\mathbf{B}^T\mathbf{v}_0. \tag{9}$$

The residuals are initialized with $\mathbf{v}_0 = 0$ and continuously updated just like the parameters. The updated residuals $\tilde{\mathbf{v}}$ are calculated according to Equation (10). After each iteration, the updated parameters $\tilde{\mathbf{x}}$ and residuals $\tilde{\mathbf{v}}$ are set as new starting values until the adjustment has converged

$$\tilde{\mathbf{v}} = \Sigma_{ll}\mathbf{B}^T\left(\mathbf{B}\Sigma_{ll}\mathbf{B}^T\right)^{-1}\left(\mathbf{w}-\mathbf{A}\Delta\tilde{\mathbf{x}}\right). \tag{10}$$

Special attention is paid to the stochastic model Σ_{ll}. An individual variance factor is set for each observation group. This allows for an empirical variance component estimation (VCE), which will be addressed in Section 4.4. In Σ_{ll} all observations are assumed to be uncorrelated, which is an often implemented simplification due to the lack of reliable correlation information. In addition, all observations within the same observation group are considered to have the same accuracy, except for the attitude angles of the direct georeferencing unit. Roll ϕ and pitch θ are assumed twice as accurate as the heading ψ. This assumption is due to the characteristics of the direct georeferencing unit (Section 2.1) but not essential for the calibration method

$$\Sigma_{ll} = \begin{bmatrix} \sigma_d^2 & & & & & & \\ & \sigma_a^2 & & & & 0 & \\ & & \sigma_{s_e}^2 & & & & \\ & & & \sigma_{r_e}^2 & & & \\ & & & & \sigma_{z_e}^2 & & \\ & 0 & & & & \Sigma_{t_{xyz}} & \\ & & & & & & \Sigma_{\phi\theta\psi} \end{bmatrix} \tag{11}$$

$$\Sigma_{t_{xyz}} = \sigma_{t_{xyz}}^2 \cdot \mathbf{Q}_{t_{xyz}} = \sigma_{t_{xyz}}^2 \cdot \begin{bmatrix} 1 & 0 & 0 \\ 0 & 1 & 0 \\ 0 & 0 & 1 \end{bmatrix} \tag{12}$$

$$\Sigma_{\phi\theta\psi} = \sigma_{\phi\theta\psi}^2 \cdot \mathbf{Q}_{\phi\theta\psi} = \sigma_{\phi\theta\psi}^2 \cdot \begin{bmatrix} 1 & 0 & 0 \\ 0 & 1 & 0 \\ 0 & 0 & 4 \end{bmatrix}. \tag{13}$$

4.4 Variance Component Estimation

The VCE is a tool to obtain empirical estimates for the variance components of the different observation groups. This is very useful because it analyzes the precision of the observations and enables to match the stochastic model with the actual level of accuracy. This leads to a better parameter estimation. The VCE is an iterative procedure, i. e. approximate values for the variance components are needed. The initial assumption often refers to generally accepted practical values or manufacturer specifications.

The basic procedure for two uncorrelated observation groups with non-overlapping variance components in the transformed Gauß Helmert model, as used within this paper, is demonstrated in the following. For a more generalized discussion, see e. g. [10, 18, 34]. The procedure starts with an initial assumption $\Sigma_{ll,0}$ for the stochastic model with a priori variance factors $\sigma_{i,0}^2$ and cofactor matrices $\mathbf{Q}_i$

$$\Sigma_{ll,0} = \sigma_{1,0}^2\begin{bmatrix}\mathbf{Q}_1 & \\ & \mathbf{0}\end{bmatrix} + \sigma_{2,0}^2\begin{bmatrix}\mathbf{0} & \\ & \mathbf{Q}_2\end{bmatrix}. \tag{14}$$

A parameter estimation is performed with this stochastic model (Section 4.3). After convergence, update factors $\kappa_{i,0}^2$ for the individual variance factors are calculated

$$\mathbf{S} = \mathbf{B}\Sigma_{ll,0}\mathbf{B}^T \tag{15}$$

$$\mathbf{M} = \mathbf{S}^{-1} - \mathbf{S}^{-1}\mathbf{A}\left(\mathbf{A}^T\mathbf{S}^{-1}\mathbf{A}\right)^{-1}\mathbf{A}^T\mathbf{S}^{-1} \tag{16}$$

$$\kappa_{i,0}^2 = \frac{\tilde{\mathbf{v}}^T\mathbf{B}^T\mathbf{S}^{-1}\left(\mathbf{B}\begin{bmatrix}\mathbf{Q}_i & \\ & \mathbf{0}\end{bmatrix}\mathbf{B}^T\right)\mathbf{S}^{-1}\mathbf{B}\tilde{\mathbf{v}}}{tr\left(\mathbf{M}\mathbf{B}\begin{bmatrix}\mathbf{Q}_i & \\ & \mathbf{0}\end{bmatrix}\mathbf{B}^T\right)}. \tag{17}$$

These are used to estimate the a posteriori variance factors $\hat{\sigma}_{i,0}^2$ to set a new stochastic model and reiterate the

parameter estimation. The iteration is run until the variance components do not change any longer, i. e. $\kappa_{i,0}^2 = 1$

$$\hat{\sigma}_{i,0}^2 = \kappa_{i,0}^2 \cdot \sigma_{i,0}^2. \tag{18}$$

In order to further improve the quality of the parameter estimation, an outlier test is carried out. This is judicious when working with laser scanner data because these often contain blunders. Therefore, standardized residuals w_i are used, which are obtained by scaling the original residuals v_i with their accuracies σ_{v_i} from Σ_{vv}. The standardized residuals are assumed to be normally distributed with zero mean and unit variance and can be checked against a quantile of the standard normal distribution $\mathcal{N}(0, 1)$ [34]

$$\Sigma_{vv} = \Sigma_{ll}\mathbf{B}^T\mathbf{M}\mathbf{B}\Sigma_{ll} \tag{19}$$

$$H_0 : w_i = \frac{v_i}{\sigma_{v_i}} \sim \mathcal{N}(0,1). \tag{20}$$

4.5 Calibration Field and Results

The geometric system calibration was carried out in a calibration field, which consisted of eight differently orientated planar surfaces. Each plane had a size of 60 cm × 90 cm and provided good reflection characteristics due to its white surface (Figure 7, left). The georeferencing of the calibration field was realized with a 3D TLS (Leica ScanStation P20), which was localized in the e-frame by using ground control points. These had previously been observed by differential GNSS for several hours. To this end, individually calibrated antennas had been used [48]. After the transformation, the residuals between the ground control points and the extracted TLS targets were below 2 mm, which illustrates the high precision of the georeferencing.

The spatial relationship between the platform and the planes is crucial for the determination of the calibration parameters. Thus, certain scanning configurations are not suitable for the determination of certain parameters. As shown in Figure 8, the plane P_1 is well-suited to determine Δx and Δy, but it is not sensitive to changes in Δz. The plane P_2 must be added to define Δz. For α, β and γ similar considerations are possible. However, this does not mean that a specific plane is not suitable for the determination of a specific parameter. Different planes can contribute to different parameters if observed from different viewpoints. Figure 8 illustrates that besides multiple viewpoints, it is also beneficial to have a great number of differently orientated planes in each scan. Both result in a strong network that allows for a reliable estimation of the calibration parameters.

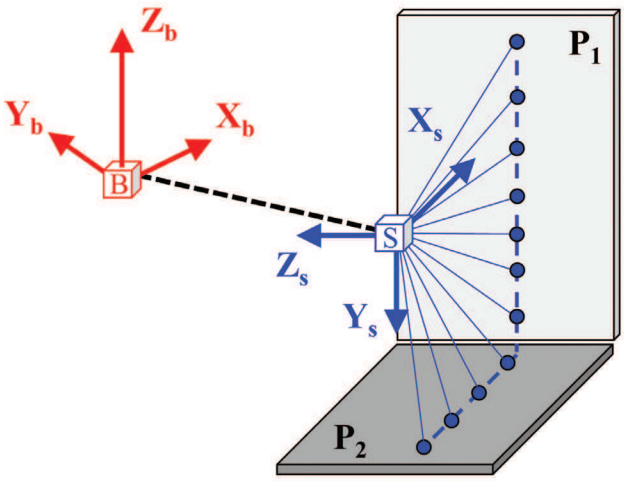

Figure 8: Different plane orientation to reliably determine all degrees of freedom, P_1 (e. g. Δx, Δy), P_2 (e. g. Δz).

In the field, the planes were statically scanned with the mobile laser scanning system from ten viewpoints with a different position and attitude of the platform. Each scan took about five minutes. The static procedure guarantees that errors in the time synchronization are irrelevant and repeated measurements lead to a reduction of random errors for the observations. The distances between the platform and the planes were kept between 2.5 m and 7.5 m to ensure both a sufficient point density on the planes and accurate 2D laser scanner readings (Figure 3). The setup was optimized in a way that always 2–6 planes were visible at the same time. After the measurement, the plane observations of the 2D laser scanner were extracted from the scanning profiles and assigned to the corresponding planar surfaces. By using the position and attitude estimates of the direct georeferencing unit and the TLS observations, the constraints of Section 4.3 can be formulated and adjusted, leading to estimates for the unknown calibration parameters.

Table 1: Estimated calibration parameters between s-frame and b-frame with associated accuracies.

Lever arms					
Δx	0.2563 m	Δy	−0.0957 m	Δz	−0.0653 m
$\sigma_{\Delta x}$	0.0043 m	$\sigma_{\Delta y}$	0.0038 m	$\sigma_{\Delta z}$	0.0041 m
Boresight angles					
α	89.5296°	β	−0.6338°	γ	119.4931°
σ_α	0.0892°	σ_β	0.0545°	σ_γ	0.1132°

The results of the system calibration are shown in Table 1. As can be seen, the accuracies of the estimated lever arms Δx, Δy and Δz are uniformly in the order of 4 mm, whereas the accuracies of the boresight angles vary slightly more in the order of 0.05° to 0.12°. Evidently, the rotation angle γ is estimated worst because this rotation turns about the z-axis of the b-frame, which usually coincides approximately with the z-axis of the n-frame. In other words, the calibration angle γ and the heading ψ are almost aligned. In Section 2.1 it has been mentioned that the heading ψ is less accurate than roll ϕ and pitch θ, and hence its inaccuracy is transferred to the angle γ. However, the accuracies of the parameters are still satisfying when taking the accuracies of the observations and the long error chain into account, starting with the 2D laser scanner and ending up with the GNSS positioning. Note, that the accuracies of the parameters are probably too optimistic due to neglected correlations between the observations.

The correlation matrix of the parameters after the adjustment confirms the high quality of the results (Figure 9). It shows a good separability of the parameters since all correlations are below 15 %. This originates from the favorable measurement setup in the calibration field.

Besides the accuracies of the estimated parameters, also the accuracy of the different observation groups is of interest because it provides an insight into the precision of the mobile laser scanning system. In addition, a correct quantification and weighting of the variances lead to a proper stochastic model, which allows for a better parameter estimation. Therefore, an empirical variance component estimation (VCE) was carried out (Table 2). Due to its iterative character, approximate a priori values are needed.

The precision of the 2D laser scanner (σ_d, σ_a) was chosen with respect to the manufacturer specification [20] and the own investigations (Section 2.2). For the TLS observations (σ_{s_e}, σ_{r_e}, σ_{z_e}) also manufacturer information

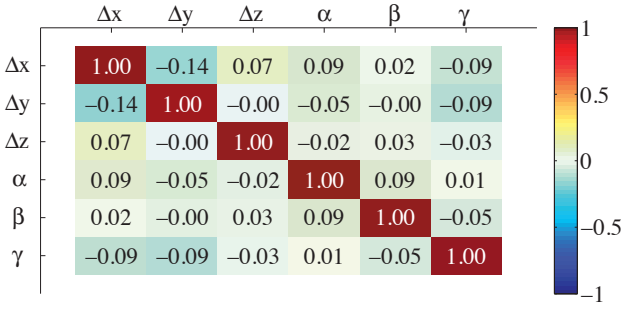

Figure 9: Correlation coefficients $\rho_{ij} = \frac{\sigma_{ij}}{\sigma_i \cdot \sigma_j}$ between the estimated calibration parameters, derived from $\Sigma_{\hat{x}\hat{x}}$.

was used [27], whereas the a priori values for the estimates of the direct georeferencing unit ($\sigma_{t_{x,y,z}}$, $\sigma_{\phi,\theta,\psi}$) are based on the studies published in [8].

Table 2: Variance component estimation (VCE) for the different observation groups.

	VC (a priori)	VC (a posteriori)
σ_d	0.0050 m	0.0008 m
σ_a	0.1000°	0.1073°
σ_{s_e}	0.0010 m	0.0011 m
σ_{r_e}	0.0025°	0.0051°
σ_{z_e}	0.0025°	0.0032°
$\sigma_{t_{xyz}}$	0.0150 m	0.0105 m
$\sigma_{\phi\theta\psi}$	0.5000°	0.1595°

Obviously, the estimated variance components of the TLS are most widely consistent with the manufacturer specification. However, the accuracy of the angles is slightly worse. This may originate from the fact that the observations contain both the accuracy of the 3D laser scanner and the georeferencing of the calibration field. The estimated accuracies of the direct georeferencing unit are in a reasonable range but better than priorly expected. This can be constituted by the fact that the planar surfaces were measured statically. In further consequence, already averaged positions and attitudes were used in the adjustment, which are considered to be more accurate than a single measurement. Note, that $\sigma_\psi = 2\,\sigma_{\phi\theta\psi}$, see Equation (13).

In contrast, the estimate of σ_d is considerably better than expected. It results from the fact that likewise not the original observations, but averaged distances for the individual angular steps were used in the adjustment (cf. red dots in Figure 5). The authors found this simplification to be feasible because it accelerates the calculations. In addition to it, the large number of 2D laser scanner observations is not incorporated as uncorrelated, which leads to a more realistic estimation for the accuracy of the parameters $\Sigma_{\hat{x}\hat{x}}$.

All estimated variance components must be considered to be too optimistic due to unmodeled correlations. This also affects the accuracy of the parameters.

5 System Evaluation

5.1 Error Propagation

In a final step, a system evaluation was performed in order to make a statement about the accuracy of the presented

mobile laser scanning system. Initially, an error propagation of Equations (1) and (2) was carried out to predict the expected accuracy σ_{3D} of a kinematically recorded 3D object point. It uses the previously estimated variance components and parameter accuracies of the system calibration (Tables 1 and 2) and the results presented in Figure 3. The latter provide more realistic estimates for the distance accuracy σ_d of the 2D laser scanner. The error propagation provides a covariance matrix $\sum_{x_e y_e z_e}$ for every single object point. Its trace is a measure for the 3D point accuracy

$$\sigma_{3D} = \sqrt{tr\left(\sum_{x_e y_e z_e}\right)} = \sqrt{\sigma^2_{x_e} + \sigma^2_{y_e} + \sigma^2_{z_e}}. \quad (21)$$

The results of the error propagation with respect to the distance *d* are outlined in Table 3. As a result, the accuracy of a 3D object point can be specified in the order of cm to dm. Because of angular deviations, the accuracy declines with increasing distance between the mobile laser scanning system and the object. For every distance, a minimum and a maximum value is stated because the covariance matrix $\sum_{x_e y_e z_e}$, and thus the 3D point accuracy σ_{3D}, varies due to the changing scanning angle *a* of the 2D laser scanner.

Table 3: Predicted 3D point accuracy σ_{3D} of the mobile laser scanning system with respect to the distance *d*.

d	σ_{3D}	*d*	σ_{3D}
1 m	2.07–2.14 cm	10 m	5.12–7.18 cm
2 m	2.22–2.46 cm	15 m	7.37–10.53 cm
3 m	2.46–2.90 cm	20 m	9.68–13.92 cm
5 m	3.09–4.00 cm	25 m	12.02–17.33 cm
7 m	3.86–5.23 cm	30 m	14.37–20.75 cm

A similar but theoretical study on the accuracy of mobile mapping systems can be found in [13]. Therein, the influences of the individual observation groups are examined in more detail. Moreover, a division into horizontal and vertical accuracy is made.

5.2 Selection of the Evaluation Method

Various methods for the evaluation of mobile laser scanning systems have been reported, which primarily make use of natural checkpoints like centers of street lights, gullies or corners of buildings [1, 16, 19, 23, 25, 38, 45], or artificial checkpoints like (spherical) laser scanner targets, regular gridded checkpoints or others [14, 23, 25, 46]. The coordinates of the checkpoints are extracted from the point clouds and compared to priorly determined reference values. This allows for an investigation of the absolute accuracy (correctness) and the relative accuracy (precision), when measuring the same checkpoints several times. However, this practice ignores major parts of the point clouds. In [17] kinematic point clouds are compared with an already existing georeferenced 3D city model. In this case, differences between point clouds and planar surfaces, which have been extracted from the model, are calculated.

Within this work, another approach was chosen, which uses the entire point cloud to evaluate the mobile laser scanning system and to verify the estimates of the error propagation (Section 5.1). For this purpose, kinematic point clouds are checked against static reference point clouds of a high-precision TLS as a whole. The Poppelsdorfer Schloss in Bonn and a machine hall in Klein-Altendorf were selected as test sites. The georeferencing of the TLS (Leica ScanStation P20) was realized by using ground control points. The accuracy of the reference point clouds can thus be specified in the order of a few mm since the measuring practice was equivalent to the georeferencing of the calibration field (Section 4.5).

Additionally, a third test site without reference values was scanned in order to test the mobile laser scanning system for its suitability in the field of application. A major part of the botanic garden in Bonn was selected to be appropriate for this kind of examination. This leads to a total of three evaluation data sets

- Poppelsdorfer Schloss (Bonn),
- Machine hall (Klein-Altendorf),
- Botanic garden (Bonn).

The comparison between the kinematic point clouds and the static reference point clouds was performed with the open source software library *CloudCompare v2.6.1* [4]. Two different kinds of comparisons were implemented

- Cloud-to-Cloud comparison (C2C),
- Cloud-to-Mesh comparison (C2M).

The first one is a direct cloud-to-cloud comparison with a local quadratic modeling on the reference point cloud. That means that not the distances between nearest neighbors are calculated, but orthogonal distances to local surface patches on the reference point cloud.

This is comparable to a cloud-to-mesh comparison, the second implemented option. The meshing of the reference point cloud is provided by a 2.5D Delaunay triangulation. For this purpose, the point cloud is projected onto its best fitting plane. Next, the received 2D points are triangulated and the 2D mesh is applied to the 3D points.

The advantage of the cloud-to-mesh comparison is that signed deviations can be derived, which are more suitable to detect systematic errors. However, the drawback of the meshing is that it is suitable for rather flat point clouds. This is only partly fulfilled due to many vertical structures inside the test sites.

5.3 Results

5.3.1 Poppelsdorfer Schloss / Klein-Altendorf

The differences δ between the kinematic point clouds and the static reference point clouds are depicted in Figures 10 (Poppelsdorfer Schloss) and 13 (Klein-Altendorf) for the C2C comparison and the C2M comparison. The differences of Figure 13 are visualized as color-coded scatter plots in Figure 12. In addition, Table 4 shows the mean, the median, the standard deviation (STD) and the root mean square error (RMS) of the histograms. Note, that for the C2C comparison only the RMS is meaningful.

The results of the comparisons show that the 3D accuracy of the mobile laser scanning system can be specified in the order of cm to dm as predicted by the error propagation (Section 5.1). Figure 10 shows that 78.2% of the points at the Poppelsdorfer Schloss differ less than 10 cm and 97.5% less than 20 cm from the reference point cloud. The results for Klein-Altendorf are even better because 85.3% of the points differ less than 5 cm and 97.8% less than 10 cm from the reference solution (Figure 13).

The parameters of the histograms (Table 4) also indicate the conformity between the predicted accuracy and the actual obtained accuracy. The standard deviation and RMS values for Klein-Altendorf are between 3.43 cm and 3.91 cm and those for the Poppelsdorfer Schloss are between 8.12 cm and 8.47 cm. The mean distances between the 2D laser scanner and the object were about 5.4 m and 11.7 m for these test sites, respectively. When visualizing the predicted accuracy values of the error propagation in Table 3 and adding the RMS values of Table 4, the conformity is clearly recognizable (Figure 11). These results indicate that the previous studies on the system accuracy can be assumed to be reasonable.

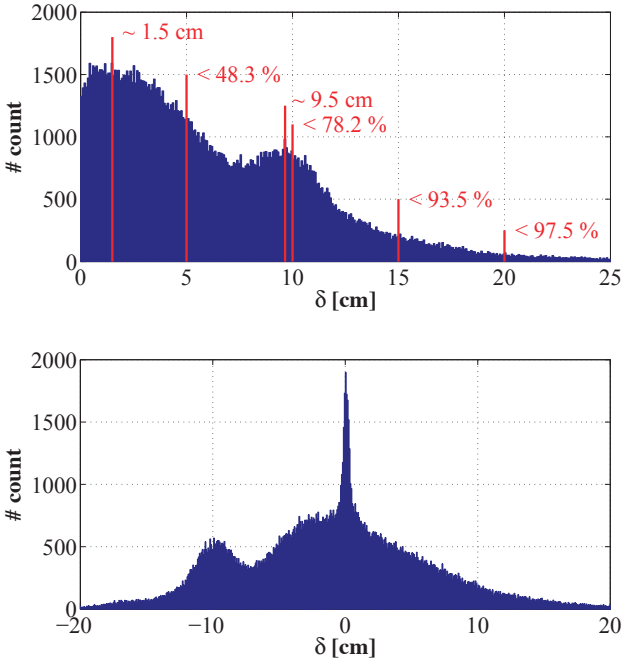

Figure 10: Deviations δ of the C2C comparison (top) and the C2M comparison (bottom) at the Poppelsdorfer Schloss.

Table 4: Parameters of the differences δ between the kinematic point clouds and the static reference point clouds (STD: standard deviation, RMS: root mean square error).

	Differences δ (C2C)	Differences δ (C2M)
	Klein-Altendorf	Klein-Altendorf
Mean	*(2.72 cm)*	0.53 cm
Median	*(1.91 cm)*	0.10 cm
STD	*(2.81 cm)*	3.43 cm
RMS	3.91 cm	3.47 cm
	Poppelsdorfer Schloss	Poppelsdorfer Schloss
Mean	*(6.53 cm)*	−1.22 cm
Median	*(5.22 cm)*	−0.80 cm
STD	*(5.41 cm)*	8.12 cm
RMS	8.47 cm	8.21 cm

However, it must be pointed out that this is only a rough inspection because of several unconsidered aspects. On the one hand, the results of the error propagation in Section 5.1 are probably too optimistic due to neglected correlations and the use of variance components which

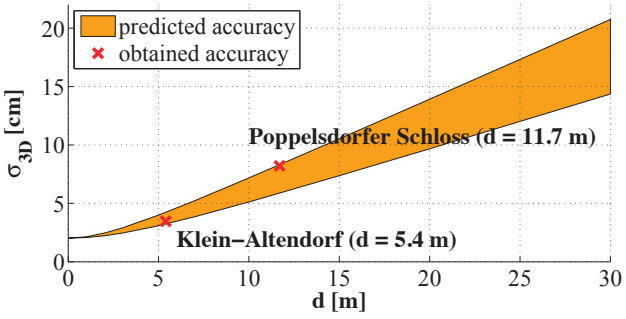

Figure 11: Predicted 3D point accuracy σ_{3D} (yellow area) and actually obtained accuracy (red crosses) of the mobile laser scanning system with respect to the distance d.

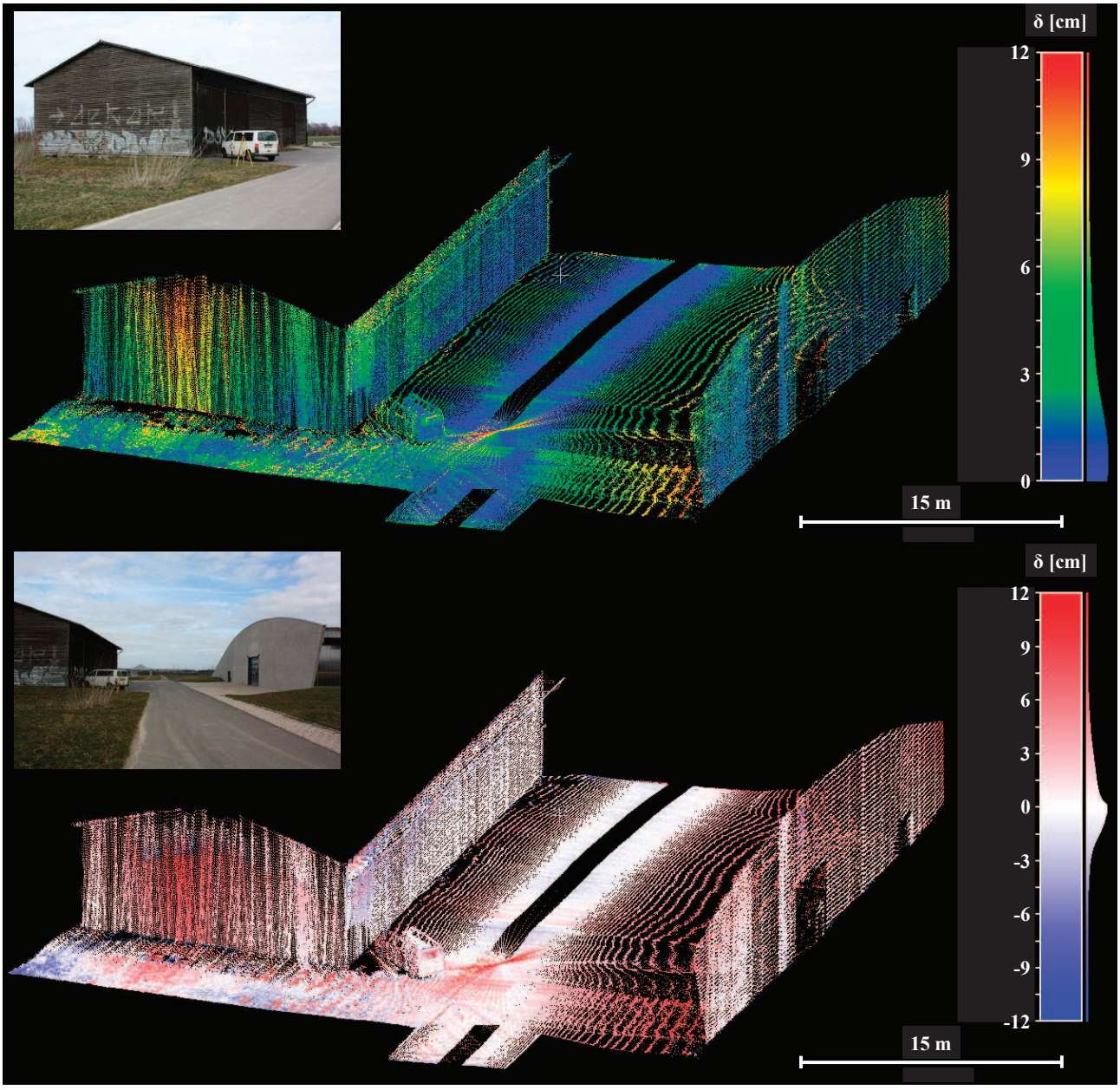

Figure 12: Kinematic scan of a machine hall in Klein-Altendorf. The picture shows the differences δ to the reference solution for the C2C comparison (top) and C2M comparison (bottom), which verify that the 3D point accuracy of the mobile laser scanning system is in the order of cm to dm.

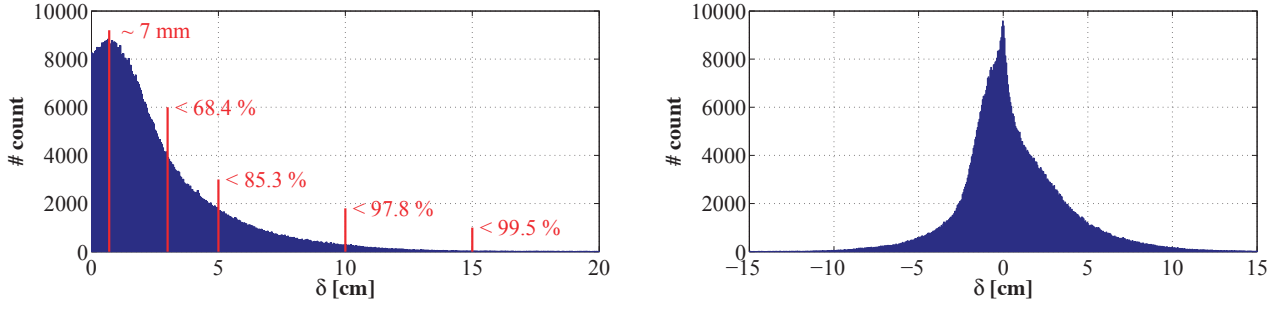

Figure 13: Deviations δ of the C2C comparison (left) and C2M comparison (right) in Klein-Altendorf. The histograms correspond to the color-coded scatter plots in Figure 12.

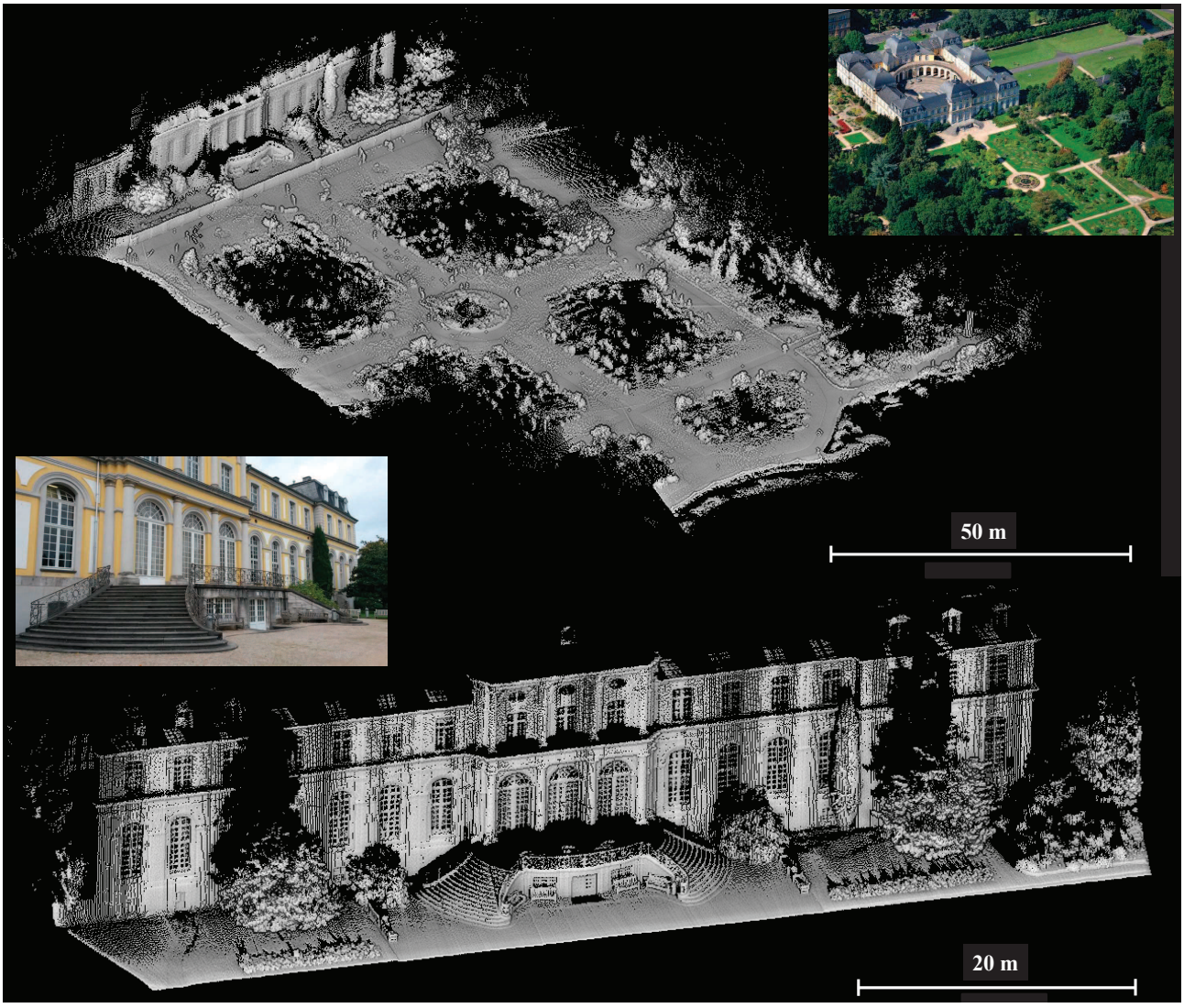

Figure 14: Kinematic scan of the botanic garden (top) and the Poppelsdorfer Schloss (bottom) in Bonn. The point clouds can be described as geometrically compact and intrinsically consistent (Picture top right: © Universität Bonn).

are based on already averaged observations. On the other hand, also the differences between the kinematic point clouds and the static reference point clouds may be too optimistic. They are received by calculating point distances to reference surfaces, and thus point displacements parallel to these surfaces cannot be detected. Finally, the RMS values of the histograms were associated with the mean distance between the 2D laser scanner and the object. To what extent this association is valid, was not questioned. Consequently, the true system accuracy must be assumed to be slightly worse than the results initially suggest. Nonetheless, it is still in the cm to dm range.

The scatter plots in Figure 12 show systematic deviations of the kinematic point cloud from the static reference point cloud. For example, the differences on the gable of the left building exceed the limit of 1 dm in a certain area, whereas the surrounding differences are significant smaller. Systematic effects can also be seen in the related histograms. The left histogram in Figure 13 shows a peak at approximately 7 mm. Moreover, the distribution in the right histogram is skewed and does not show the shape of a Gaussian distribution. This is also proved by the mean of 0.53 cm and median of 0.10 cm (Table 4), which differ from zero. The scan at the Poppelsdorfer Schloss shows a similar behavior. Figure 10 shows peaks at approximately 1.5 cm and 9.5 cm and the bottom histogram is not normally distributed. The mean of –1.22 cm and the median of –0.80 cm differ from zero as well. The reasons for these findings could not be clearly identified. Most likely, they can be traced back to the trajectory, e. g. systematic errors

in the GPS position due to changing multipath or shadowing. But also the uncompensated systematic effects of the 2D laser scanner (Section 2.2) or the system calibration might have an impact.

5.3.2 Botanic Garden

To test the mobile laser scanning system in the field of application, a larger area (approximately 7,500 m^2) of the botanic garden in Bonn was scanned kinematically. The results are shown in Figure 14. In this case, no reference solution for an evaluation was available. However, the point cloud can be described as geometrically compact and intrinsically consistent, which testifies a good long-term stability of the system. To validate this, all parts of the test site were scanned several times, showing only small displacements in the overlapping point clouds. The measurement took about 55 minutes, producing a point cloud of 6.2 million points. Including the time for the installation/demounting of the own GPS reference station (absolute position via SAPOS) and for the start-up/shut-down of the mobile laser scanning system, a total measuring time of approximately 90 minutes resulted. No ground control points or time-consuming post processing steps for the georeferencing were required.

6 Conclusion and Outlook

In this paper, a portable laser scanning system has been presented, which consists of a small, lightweight, real-time capable direct georeferencing unit and a compact, low-cost 2D laser scanner. Besides the system design and the time synchronization, a special emphasis has been placed on the geometric system calibration and the evaluation.

In the course of the calibration, the lever arms and boresight angles between the 2D laser scanner and the direct georeferencing unit could be determined with an accuracy in the order of mm and one-tenth of a degree. To this end, a special calibration technique was chosen, which utilizes identity conditions between georeferenced planar surfaces and directly georeferenced scanning profiles of the mobile laser scanning system. The results are satisfying when taking the accuracies of the observations into account.

The evaluation of the entire system brought good results, too. The deviations from reference point clouds match well with the priorly predicted accuracy, which was derived from an error propagation of empirical variance components and estimated accuracies for the calibration parameters. As a result, the 3D point accuracy of the kinematic point clouds is in the order of cm to dm, depending on the distance between the 2D laser scanner and the object.

Nonetheless, there is potential for future improvements. The calibration is time-consuming because the calibration field has to be rebuilt and georeferenced every time a system calibration is required. Moreover, the point clouds show remaining systematic errors whose origin could not be clearly identified. Therefore, the authors are currently working on the construction of a permanently installed test field for mobile mapping systems to answer the purposes of both calibration and evaluation. The focus will be on the

- optimization of the existing calibration method: plane geometry, other geometric shapes, measurement setup,
- determination of intrinsic calibration parameters,
- examination of time synchronization and trajectory,
- kinematic calibration and automatization (*on-the-fly*).

The 2D laser scanner also provides previously unexploited intensity values and is equipped with multi-echo technology, which means that multiple echoes can be received for each emitted laser beam. This improves the reliability in the cases of multiple reflections, e. g. at object edges, transparent materials, smoke, fog or vegetation, and yields an advantage over visual sensors such as cameras [5].

References

[1] Barber, D., Mills, J. and Smith-Voysey, S., Geometric validation of a ground-based mobile laser scanning system, *ISPRS Journal of Photogrammetry and Remote Sensing* **63** (2008), 128–141.

[2] Besl, P. J. and McKay, N. D., A Method for Registration of 3-D Shapes, *IEEE Transactions on Pattern Analysis and Machine Intelligence* **14** (1992), 239–256.

[3] Caruso, M. J., Applications of Magnetic Sensors for Low Cost Compass Systems, *IEEE Position, Location and Navigation Symposium* (2000), 177–184.

[4] CloudCompare, *CloudCompare – 3D Point Cloud and Mesh Processing Software, Open Source Project,* 2015, URL: http://www.cloudcompare.org (accessed June 1, 2015).

[5] Djuricic, A. and Jutzi, B., Supporting UAVs in Low Visibility Conditions by Multiple-Pulse Laser Scanning Devices, *ISPRS International Archives of the Photogrammetry, Remote Sensing and Spatial Information Sciences, Volume XL-1/W1* (2013), 93–98.

[6] Dorndorf, A., Hartmann, J., Paffenholz, J.-A., Neumann, I. and Hesse, C., Validierung und Kalibrierung eines TLS-basierten

Multi-Sensor-Systems, *Photogrammetrie Laserscanning Optische 3D-Messtechnik – Beiträge der Oldenburger 3D-Tage 2015 (Hrsg. Luhmann/Müller)* (2015), 85–97.

[7] Eling, C., Klingbeil, L. and Kuhlmann, H., Development of an RTK-GPS system for precise real-time positioning of lightweight UAVs, *Ingenieurvermessungskurs 2014, Zürich, Schweiz* **2014** (2014), 111–123.

[8] Eling, C., Klingbeil, L., Wieland, M. and Kuhlmann, H., Direct Georeferencing of Micro Aerial Vehicles – System Design, System Calibration and First Evaluation Tests, *Photogrammetrie Fernerkundung Geoinformation (PFG)* **2014** (2014), 227–237.

[9] Eling, C., Zeimetz, P. and Kuhlmann, H., Development of an instantaneous GNSS/MEMS attitude determination system, *GPS Solutions* **2013** (2013), 129–138.

[10] Förstner, W., Ein Verfahren zur Schätzung von Varianz- und Kovarianzkomponenten, *Allgemeine Vermessungs-Nachrichten (AVN)* **86** (1979), 446–453.

[11] Frei, E. A., Vennegeerts, H. and Omelanowsky, D., Kinematische Scanlösungen von p3d systems, *Terrestrisches Laserscanning 2013, DVW Schriftenreihe Band 72* (2013), 107–124.

[12] Friess, P., Toward a rigorous methodology for airborne laser mapping, *Proceedings of the International Calibration and Validation Workshop EURO COW, Castelldefels, Spain* (2006).

[13] Glennie, C., Rigorous 3D error analysis of kinematic scanning LIDAR systems, *Journal of Applied Geodesy* **1** (2007), 147–157.

[14] Glennie, C., Brooks, B., Ericksen, T., Hauser, D., Hudnut, K., Foster, J. and Avery, J., Compact Multipurpose Mobile Laser Scanning System – Initial Tests and Results, *Remote Sensing* **5** (2013), 521–538.

[15] Gräfe, G., High precision kinematic surveying with laser scanners, *Journal of Applied Geodesy* **1** (2007), 185–199.

[16] Gräfe, G, *Kinematische Anwendungen von Laserscannern im Straßenraum,* Ph.D. thesis, Gottfried Wilhelm Leibniz Universität Hannover, Fakultät für Bauingenieurwesen und Geodäsie, 2007.

[17] Haala, N., Peter, M., Kremer, J. and Hunter, G., Mobile LIDAR mapping for 3D point cloud collection in urban areas – A performance test, *The International Archives of the Photogrammetry, Remote Sensing and Spatial Information Sciences* **37** (2008), 1119–1127.

[18] Heiker, A., *Mutual validation of Earth orientation parameters, geophysical excitation functions and second degree gravity field coefficients,* Ph.d. thesis, Gottfried Wilhelm Leibniz Universität Hannover, Fakultät für Bauingenieurwesen und Geodäsie, 2013.

[19] Hesse, C., *Hochauflösende kinematische Objekterfassung mit terrestrischen Laserscannern,* Ph.D. thesis, Gottfried Wilhelm Leibniz Universität Hannover, Fakultät für Bauingenieurwesen und Geodäsie, 2007.

[20] Hokuyo Automatic Co., Ltd., *Hokuyo UTM-30LX-EW Specifications,* 2012, URL: http://www.hokuyo-aut.jp/02sensor/07scanner/download/products/utm-30lx-ew/ (accessed April 1, 2015).

[21] Holst, C., Artz, T. and Kuhlmann, H., Biased and unbiased estimates based on laser scans of surfaces with unknown deformations, *Journal of Applied Geodesy* **8** (2014), 169–184.

[22] Joeckel, R., Stober, M. and Huep, W., *Elektronische Entfernungs- und Richtungsmessung und ihre Integration in aktuelle Positionierungsverfahren (5. Auflage),* Wichmann, 2008.

[23] Kaartinen, H., Hyyppä, J., Kukko, A., Jaakkola, A. and Hyyppä, H., Benchmarking the Performance of Mobile Laser Scanning Systems Using a Permanent Test Field, *Sensors* **12** (2012), 12814–12835.

[24] Keller, F. and Sternberg, H., Multi-Sensor Platform for Indoor Mobile Mapping: System Calibration and Using a Total Station for Indoor Applications, *Remote Sensing* **5** (2013), 5805–5824.

[25] Kukko, A., Kaartinen, H., Hyyppä, J. and Chen, Y., Multiplatform Mobile Laser Scanning: Usability and Performance, *Sensors* **12** (2012), 11712–11733.

[26] Le Scouarnec, R., Touzé, T., Lacambre, J. B. and Seube, N., A positioning free calibration method for mobile laser scanning applications, *Proceedings of the ISPRS Workshop on Laser Scanning, Antalya, Turkey* (2013), 157–162.

[27] Leica Geosystems AG, *Leica ScanStation P20, Product Specifications,* 2013, URL: http://www.leica-geosystems.com (accessed April 28, 2015).

[28] Lenzmann, L. and Lenzmann, E., Strenge Auswertung des nichtlinearen Gauß-Helmert-Modells, *Allgemeine Vermessungs-Nachrichten (AVN)* **111** (2004), 68–73.

[29] Lindenthal, S. M., Ussyshkin, V. R., Wang, J. G. and Pokorny, M., Airborne LIDAR: A fully-automated self-calibration procedure, *The International Archives of the Photogrammetry, Remote Sensing and Spatial Information Sciences, Volume XXXVIII-5/W12* (2011), 73–78.

[30] Maddern, W., Harrison, A. and Newman, P., Lost in Translation (and Rotation): Rapid Extrinsic Calibration for 2D and 3D LIDARs, *IEEE International Conference on Robotics and Automation (ICRA)* (2012), 3096–3102.

[31] Mikhail, E. M. and Ackermann, F. E., *Observations and Least Squares,* Dun-Donnelley, 1976.

[32] Neitzel, F., Generalization of total least-squares on example of unweighted and weighted 2D similarity transformation, *Journal of Geodesy* **84** (2010), 751–762.

[33] Neitzel, F. and Neumann, I., Scanning in Motion – Kinematisches TLS mittels mobiler Plattformen, *Terrestrisches Laserscanning 2013, DVW Schriftenreihe Band 72* (2013), 89–106.

[34] Niemeier, W., *Ausgleichungsrechnung – Statistische Auswertemethoden (2. Auflage),* de Gruyter, 2008.

[35] Odijk, D., Traugott, J., Sachs, G, Montenbruck, O. and Tiberius, C., Two Approaches to Precise Kinematic GPS Positioning with Miniaturized L1 Receivers, *Proceedings of the 20th International Technical Meeting of the Satellite Division of the Institute of Navigation (ION GNSS)* (2007), 827–838.

[36] Paffenholz, J.-A., *Direct geo-referencing of 3D point clouds with 3D positioning sensors,* Ph.D. thesis, Gottfried Wilhelm Leibniz Universität Hannover, Fakultät für Bauingenieurwesen und Geodäsie, 2012.

[37] Rieger, P., Studnicka, N., Pfennigbauer, M. and Zach, G., Boresight alignment method for mobile laser scanning systems, *Journal of Applied Geodesy* **4** (2010), 13–21.

[38] Schlichting, A., Brenner, C. and Schön, S., Bewertung von Inertial/GNSS-Modulen mittels Laserscannern und bekannter Landmarken, *Photogrammetrie, Fernerkundung, Geoinformation (PFG)* **2014** (2014), 5–15.

[39] Sheehan, M., Harrison, A. and Newman, P., Self-Calibration for a 3D Laser, *The International Journal of Robotics Research* (2011).

[40] Skaloud, J. and Lichti, D., Rigorous approach to bore-sight self-calibration in airborne laser scanning, *ISPRS Journal of Photogrammetry and Remote Sensing* **61** (2006), 47–59.
[41] Sternberg, H., Keller, F. and Willemsen, T., Precise indoor mapping as a basis for coarse indoor navigation, *Journal of Applied Geodesy* **7** (2013), 231–246.
[42] Strübing, T. and Neumann, I., Positions- und Orientierungsschätzung von LIDAR-Sensoren auf Multisensorplattformen, *Zeitschrift für Geodäsie, Geoinformation und Landmanagement (ZfV)* **138** (2013), 210–221.
[43] Talaya, J., Alamus, R., Bosch, E., Serra, A., Kornus, W. and Baron, A., Integration of a terrestrial laser scanner with GPS/IMU orientation sensors, *Proceedings of the 20th ISPRS Congress* (2004).
[44] Teixidó, M., Pallejà, T., Font, D., Tresanchez, M., Moreno, J. and Palacín, J., Two-Dimensional Radial Laser Scanning for Circular Marker Detection and External Mobile Robot Tracking, *Sensors* **12** (2012), 16482–16497.
[45] Vennegeerts, H., *Objektraumgestützte kinematische Georeferenzierung für Mobile-Mapping-Systeme,* Ph.D. thesis, Gottfried Wilhelm Leibniz Universität Hannover, Fakultät für Bauingenieurwesen und Geodäsie, 2011.
[46] Vennegeerts, H., Martin, J., Becker, M. and Kutterer, H., Validation of a kinematic laserscanning system, *Journal of Applied Geodesy* **2** (2008), 79–84.
[47] Wolf, H., *Ausgleichungsrechnung – Formeln zur praktischen Anwendung,* Dümmler, 1975.
[48] Zeimetz, P., *Zur Entwicklung und Bewertung der absoluten GNSS-Antennenkalibrierung im HF-Labor,* Ph.D. thesis, Rheinische Friedrich-Wilhlems Universität Bonn, Institut für Geodäsie und Geoinformation, 2010.